

Forecasting Response to Treatment with Global Deep Learning and Patient-Specific Pharmacokinetic Priors

Willa Potosnak
Cristian Challu
Kin G. Olivares
Artur Dubrawski

WPOTOSNA@CS.CMU.EDU
CCHALLU@CS.CMU.EDU
KDGUTIER@CS.CMU.EDU
AWD@CS.CMU.EDU

Auton Lab, School of Computer Science, Carnegie Mellon University, Pittsburgh, PA, USA

Abstract

Forecasting healthcare time series is crucial for early detection of adverse outcomes and for patient monitoring. Forecasting, however, can be difficult in practice due to noisy and intermittent data. The challenges are often exacerbated by change points induced via extrinsic factors, such as the administration of medication. To address these challenges, we propose a novel hybrid global-local architecture and a pharmacokinetic encoder that informs deep learning models of patient-specific treatment effects. We showcase the efficacy of our approach in achieving significant accuracy gains for a blood glucose forecasting task using both realistically simulated and real-world data. Our global-local architecture improves over patient-specific models by 9.2-14.6%. Additionally, our pharmacokinetic encoder improves over alternative encoding techniques by 4.4% on simulated data and 2.1% on real-world data. The proposed approach can have multiple beneficial applications in clinical practice, such as issuing early warnings about unexpected treatment responses, or helping to characterize patient-specific treatment effects in terms of drug absorption and elimination characteristics.

Keywords: Multi-Input Forecasting, Glucose, Pharmacokinetics, Deep Learning

1. Introduction

Forecasting healthcare time series is crucial for early detection of adverse outcomes and patient monitoring (Churpek et al., 2016; Gerry et al., 2020). Notably, healthcare time series data are often affected by exogenous factors, such as medication, exercise, or diet. Accurate forecasting systems should strive to harness the predictive potential of these factors.

While the inclusion of exogenous variables can significantly enhance prediction accuracy (Olivares et al., 2022a), there are instances in which their integration yields minimal to no improvement (McShinsky and Marshall, 2020; Rubin-Falcone et al., 2020).

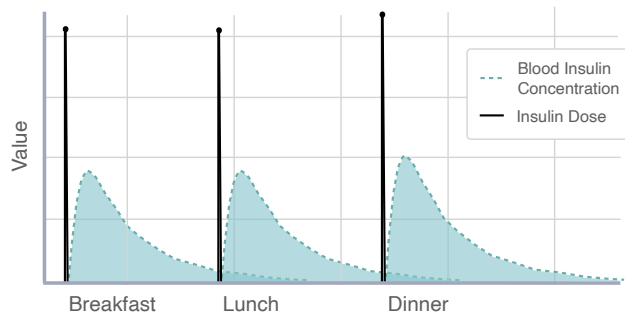


Figure 1: Insulin dose is usually known and recorded in data, whereas plasma insulin concentration is unobservable and subject to changes over time.

Leveraging the predictive power of exogenous variables presents unique challenges, especially in healthcare, where patient signals and exogenous factors, such as medication dose, often exhibit a temporal resolution mismatch. Furthermore, while the medication dose is usually known, we cannot directly observe the drug absorption and elimination parameters or plasma concentration of the drug, as illustrated in Fig. 1. Consequently, their impact on the predictive signal remains hidden.

We consider the blood glucose forecasting task while taking into account hidden medication effects. In our data, blood glucose measurements are taken every five minutes, and exogenous variables such as

carbohydrate ingestion or application of insulin are recorded as instantaneous points in time. To model hidden temporal effects of such exogenous events, we propose to modify contemporary deep learning forecasting models by adding a pharmacokinetic encoder. The encoder leverages pharmacokinetic knowledge to generate patient-specific plasma insulin concentration profiles. In our framework, global parameters of a forecasting architecture are shared across multiple patients (Semenoglou et al., 2021), but the parameters of the encoder are learned from the individual patient’s historical data to address inter-subject variability in response to treatment.

The main contributions of this paper are:

- **Pharmacokinetic Encoder.** We introduce a novel architecture module that generates plasma drug concentration profiles to capture time-dependent medication treatment effects.
- **Hybrid Global-Local Architecture.** We bolster global architectures (with parameters shared across patients) with a learnable patient-specific pharmacokinetic encoder.
- **State-of-the-Art Results.** We obtain significant accuracy improvements on a large scale simulated and real-world blood glucose forecasting datasets.

1.1. Glucose Forecast Background

Type I diabetes (T1DM) patients must regularly monitor and regulate their blood glucose values to prevent hypoglycemic or hyperglycemic events, which can drastically impact organs or even be fatal. Insulin dosages, T1DM’s most crucial treatment, are represented as instantaneous events in data, which can hide their long-lasting effects. Effectively capturing the dynamic effects of medication over time is crucial to accurately predict the impact of insulin on blood glucose.

Pharmacokinetic modeling is a natural solution to the aforementioned problem, as it can unveil medication effects through knowledge of drug movement through the body. For example, pharmacokinetics provides a well-established understanding of plasma insulin concentration changes over time based on drug absorption and elimination characteristics (Binder et al., 1984; Rubin-Falcone et al., 2022).

For extravascular injections, the plasma concentration-time profile exhibits right-skewed

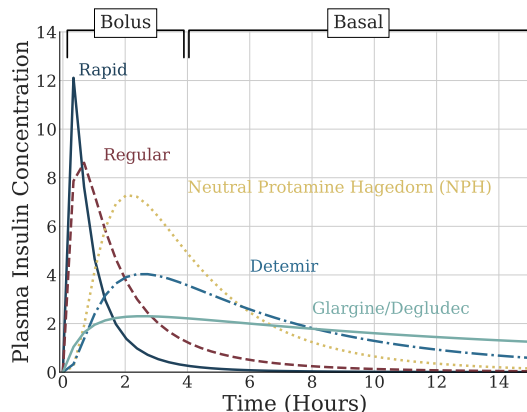


Figure 2: Pharmacokinetic modeling of plasma insulin concentration over time.

characteristics (Rosenbaum, 2017). Fig. 2 depicts pharmacokinetic modeling of plasma insulin concentration over time for different bolus and basal insulin types. Generally, bolus doses are quick-acting and, thus, often taken before meals compared to basal insulin, which is longer-acting and serves to regulate blood glucose levels throughout the day.

In Fig. 2, the area under the concentration curve measures drug *bioavailability*, the fraction of the absorbed dose that reaches the intended site of systemic circulation intact. Bioavailability can vary based on many factors, including type of medication, dosage, and patient-specific characteristics. For instance, the bioavailability of an intravenous dose of any drug is close to 100 percent (Søeborg et al., 2012). However, for subcutaneous injections, bioavailability is lower due to unintended drug absorption or elimination.

1.2. Previous Work

Neural Forecasting. In recent years, neural networks have demonstrated significant improvements compared to traditional forecasting algorithms, following the adoption of the cross-learning technique (Smyl, 2019; Semenoglou et al., 2021), which involves utilizing expressive global models to leverage data from vast collections of related time series.

The success of this global modeling approach has seen deep forecasting methods become ubiquitous in industrial forecasting systems (Wen et al., 2017; Lim et al., 2021), and in academia (Oreshkin et al., 2020).

Glucose Forecasting. Neural Forecasting literature has permeated into the field of glucose level

prediction, outperforming the accuracy of classic statistical methods (Xie and Wang, 2020). Past research includes various neural network designs ranging from *Multi Layer Perceptrons* (MLP; Jahangir et al. 2017), *Recurrent Neural Networks* (RNN; Fox et al. 2018; Rabby et al. 2021; Rubin-Falcone et al. 2022) to *Temporal Convolutional Networks* (TCN; Li et al. 2019).

Despite recent advancements in glucose forecasting, two significant challenges remain. Firstly, existing architectures struggle to effectively utilize sparse exogenous variables with the exception of Rubin-Falcone et al. (2022). Medication and carbohydrate values are recorded as sparse values in data, which may contribute to model difficulty in learning the effects of treatment on blood glucose levels. Early solutions propose summing up exogenous values to the current point within an input window to replace sparse features as shown in Fig. 3. However, this “sum-total” preprocessing approach fails to capture time-dependent changes in medication, which can be achieved through pharmacokinetic modeling of plasma insulin concentration. Despite this, deep learning methods used to forecast blood glucose do not consider pharmacokinetics to inform model training. Secondly, many studies (Xie and Wang, 2020; Rubin-Falcone et al., 2022; Zaidi et al., 2021) rely on individualized networks for each patient, with limited adoption of cross-learning approaches that could enhance forecasting models by leveraging shared knowledge across patients. Our proposed approach address both challenges in a novel hybrid global-local modeling approach that learns patient-specific pharmacokinetics to improve deep learning model capabilities in forecasting blood glucose levels.

2. Cohort

Simulated data An open-source python implementation of the FDA-approved UVa/Padova Simulator (2008 version) (Xie, 2018; Visentin et al., 2016) provides clinical and biological parameters for 30 patients (10 adults, 10 adolescents, and 10 children) with Type-I diabetes. Clinical parameters include information on age and weight, and biological parameters include information on insulin-glucose kinetics, such as absorption constants. We generate 54 days of data for each patient to match the median training set of the OhioT1DM, and approximately 9 days for the test set. In a similar approach to (Rubin-Falcone et al., 2022), the meal schedule used to generate simu-

lated data was based on the Harrison-Benedict equation (Arthur Harris and Gano Benedict, 21919) with approximately 3 meals per day and no additional snacks. Height data was not provided in the patient parameters, and so was estimated at 140cm, 170cm, and 175cm for adults, adolescents, and children, respectively.

The ‘Dexcom’ continuous glucose monitor (CGM) option was used to obtain glucose readings at 5-minute intervals. The default basal-bolus controller provided in the simulation was used to administer insulin at the time of each meal, where the bolus amount is computed based on the current glucose level, the target glucose level, the patient’s correction factor, and the patient’s carbohydrate ratio. However, we adapt the controller to deliver basal doses once per hour, consistent with the OhioT1DM dataset. The resulting simulated data consists of CGM (in mg/dL) values, insulin rate (in units per minute), and carbohydrates (in grams), referred to as CHO. We extract the bolus insulin rate from the overall insulin rate as the difference in the continuous basal insulin rate, which is consistent hourly doses. Blood glucose time series for 6 simulated patients are shown in Fig. 7 in Appendix A.1.

OhioT1DM 12 de-identified individuals with Type 1 diabetes are included in the OhioT1DM 2018 and 2020 datasets (Marling and Bunescu, 2020). Each patient has approximately 8 weeks of data that includes blood glucose (mg/dL) measurements recorded with a CGM at a frequency of 5-minutes. The dataset consists of both female (n=5) and male (n=8) subjects with unspecified ages within the ranges of 20-40, 40-60, and 60-80. Information on insulin pump model and type of insulin is also provided.

Sparse exogenous features in the data include basal rate (in units per hour), temporary basal rate (units per hour), and bolus insulin (units), and CHO values. Bolus insulin consists of both ‘normal’ insulin, which is recorded as an instantaneous administration, and ‘square dual’, where the insulin dose is stretched over a defined period. ‘Square dual’ insulin doses were divided evenly across the specified administration window with the assumption that insulin units are administered consistently across specified timestamps. If multiple bolus administrations occurred within the same minute, the insulin units were summed. Basal insulin was included as hourly doses. For timestamps with overlapping basal rates, the last basal rate value

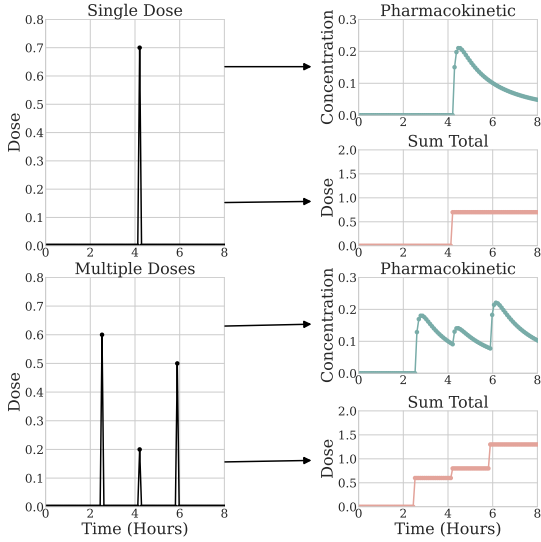


Figure 3: Instantaneous medication administrations are represented as sparse variables in time series data. We propose a Pharmacokinetic featurization alternative to encapsulate the relative time-dependent effects of sparse medication variables.

was considered. When specified, the temporary basal rate superseded the basal rate.

We use the specified train and test partitions provided in the dataset. The maximum number of test samples consistent across all patients (2691 samples) was used to obtain equal test sets of approximately 9 days. The sample count and percent missing data for each subject are included in Table 2 in Appendix A.1. Missing values were forward filled to prevent data leakage. Blood glucose time series plots for 6 subjects are shown in Fig. 8 in Appendix A.1.

3. Methods

We aim to forecast blood glucose levels 30 minutes into the future consistent with prior work (Rubin-Falcone et al., 2022; Xie and Wang, 2020), based on a 10 hour history of blood glucose, carbohydrate, insulin basal, and insulin bolus values.

3.1. Pharmacokinetic Encoder

We propose a novel pharmacokinetic encoder that informs deep learning models of time-dependent plasma drug concentration to enable more accurate

forecasting of treatment outcomes. The encoder consists of a function, C , that takes in sparse exogenous medication variables and generates a concentration-time profile for a specified dose, d , using the following equation:

$$C(t, d, k_a^{(i)}) = \frac{d}{tk_a^{(i)}\sqrt{2\pi}} \exp\left\{-\frac{1}{2(k_a^{(i)})^2}(\log(t) - 1)^2\right\} \quad (1)$$

where t is the time and $k_a^{(i)}$ is the absorption rate constant for patient, i . Here, C is equivalent to the log-normal probability density function (pdf) with $\sigma = k_a$ and $\mu = 1$ and a scaling factor, d . Concentration profiles are generated under the assumption that all insulin administrations adhere to 100% bioavailability. As bioavailability equates to the area under the concentration curve, the scaled curve thus integrates to the specified dose, d .

Let N be the number of subjects in the data. The absorption rate constant, $k_{a_{\text{bolus}}} \in [0, 1]^{Nx1}$ and $k_{a_{\text{basal}}} \in [0, 1]^{Nx1}$ are represented as network embedding weights that are initialized between values of 0 and 1 prior to model training. Initial $k_{a_{\text{bolus}}}$ and $k_{a_{\text{basal}}}$ values are tuned as model hyperparameters. During model training, sparse basal and bolus features are passed into the pharmacokinetic encoder along with their respective $k_a^{(i)}$ parameters, as shown in Fig. 4. The encoder then replaces sparse medication features in the training window with the corresponding concentration curve. Non-medication features, such as CHO, are unaffected. For each training step, $k_{a_{\text{bolus}}}^{(i)}$ and $k_{a_{\text{basal}}}^{(i)}$ are updated for each patient, i , with gradient descent optimization.

Multiple insulin doses may occur at close intervals in an event often referred to as “insulin stacking” as shown in Fig. 3. The encoder leverages a matrix, $W \in \mathbb{R}^{L \times L}$, where L refers to the lag time, to perform vectorized operations that enable generating concentration curves for multiple doses in an input window in $\mathcal{O}(1)$ time. Each row of W represents a time count up to the input time where the count shifts one time step for each subsequent row. Concentration curves are generated for each row of W using the dose at the corresponding time index. The final concentration curve feature, which can reflect the impact of multiple doses, is generated by aggregating the individual concentration curves across time steps.

$$W = \begin{bmatrix} 0 & 1 & 2 & 3 & \cdots & L-1 \\ 0 & 0 & 1 & 2 & \cdots & L-2 \\ \cdots & \cdots & \cdots & \cdots & \cdots & \cdots \\ 0 & 0 & 0 & 0 & \cdots & 0 \end{bmatrix} \in \mathbb{R}^{L \times L} \quad (2)$$

$$x'_{bolus}{}^z = \sum_{t=0}^L C(W_{t,j} \cdot f, x'_{t,bolus}{}^z, k_{a_{bolus}}^{(i)}) \quad (3)$$

$$x'_{basal}{}^z = \sum_{t=0}^L C(W_{t,j} \cdot f, x'_{t,basal}{}^z, k_{a_{basal}}^{(i)}) \quad (4)$$

Here, $x \in \mathbb{R}^{L \times 1}$ a sparse exogenous variable, where x_{bolus} and x_{basal} correspond to bolus and basal insulin doses, respectively. Additionally, $f \in \mathbb{R}$ is the frequency of the data and $x'^z \in \mathbb{R}^{1 \times L}$ is the new plasma insulin concentration feature.

For each time step within the forecast horizon, H , forecasts, \hat{y} , are generated by the model f_θ as a function of concentration curves, x' , other non-medication time series, x , and static features s ,

$$\hat{y}_{t:t+H}^z = f_\theta(y_{t-L:t}^z, x'_{t-L:t}{}^z, x_{t-L:t}^z, s^z). \quad (5)$$

In the proposed context, $x'_{t-L:t}$ consists of x'_{basal} and x'_{bolus} , x consists of x_{CHO} , and s consists includes patient age, weight, one-hot encoded subject identification number, and insulin pump type, if applicable.

3.2. Models

To assess forecasting performance across various model architectures, we trained models with six different algorithms as baselines. The implementations of these models were obtained from the `Neuralforecast` (Olivares et al., 2022b) and `StatsForecast` (Garza et al., 2022) libraries. More information on these models is provided in Appendix A.2.

Statistical Model We employed Exponential Smoothing (ETS; Hyndman 2008) as our statistical baseline model.

Deep Learning Models Our deep learning baselines included the following models: Multi-Layer Perceptron (MLP; Rosenblatt 1958), NBEATS/NHITS Oreshkin et al. (2020); Challu et al. (2022), Recurrent Neural Network (RNN; Elman (1990); Cho et al. (2014)), Long-Short Term Memory (LSTM; Sak et al. (2014)), Temporal Convolution Network with an MLP

Decoder (TCN; Bai et al. (2018); van den Oord et al. (2016)), and Temporal Fusion Transformer (TFT; Lim et al. (2021))

In contrast to previous efforts that focused on training models for individual subjects, or *local* models, we employ *global* architectures with parameters shared across subjects Rubin-Falcone et al. (2022); Xie and Wang (2020). For each dataset, models were trained using all patient data to generate one global model that was applied across patients. We showcase the efficacy of global architectures in producing improved forecasts by training local models for comparison against our global model. Moreover, apart from reducing computational and storage costs, global models could prove more applicable in real-world scenarios since they can be utilized for new patients with limited or no available training data.

Models were trained using Adam optimizer (Kingma and Ba, 2017). Optimal hyperparameters were selected based on a validation set with cross-validation. Model hyperparameters that minimized Huber loss across all time points in the prediction horizon of the validation set were selected. Huber estimator was selected as a robust loss function, \mathcal{L} , given its ability to reduce the impact of outliers and offer more stable results compared to other functions:

$$\mathcal{L}(y, \hat{y}, \delta) = \begin{cases} \frac{1}{2}(y - \hat{y})^2, & \text{if } |y - \hat{y}| \leq \delta, \\ \delta \cdot (|y - \hat{y}| - \frac{1}{2}\delta), & \text{otherwise.} \end{cases} \quad (6)$$

Given the use of forward-filling to account for missing values in the OhioT1DM dataset, timestamps with forward-filled values were omitted from the validation set. The deep learning models were trained using an NVIDIA A100 Tensor Core GPU.

3.3. Baselines

We implement three baselines against which we compare our proposed hybrid global-local architecture and pharmacokinetic encoder approach:

Univariate signal We train models using the univariate blood glucose signal and static features to provide forecast.

Univariate signal with exogenous features We train models on the univariate blood glucose signal, static features, and exogenous features, consisting of sparse basal and bolus insulin dose values.

Univariate signal with sum-total feature engineering We train models on the univariate blood

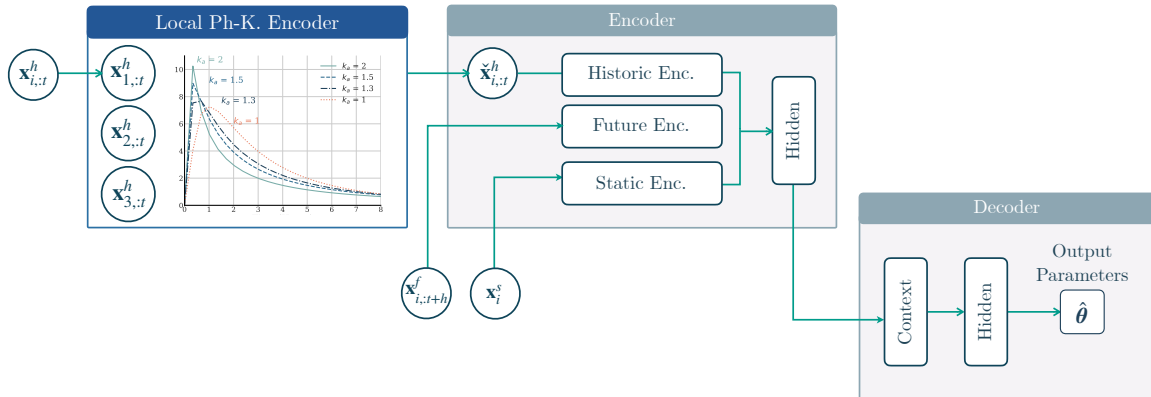


Figure 4: Hybrid Global-Local architecture. Global architectures with parameters shared across patients’ time series with local parameters from a patient-specific pharmacokinetic (Ph-K.) encoder. Sparse medication dose time series are passed into the pharmacokinetic encoder along with their respective k_a parameters to generate concentration curves. Concentration curves are then passed into a deep learning model which learns relevant hidden states (hidden) and output parameters, $\hat{\theta}$.

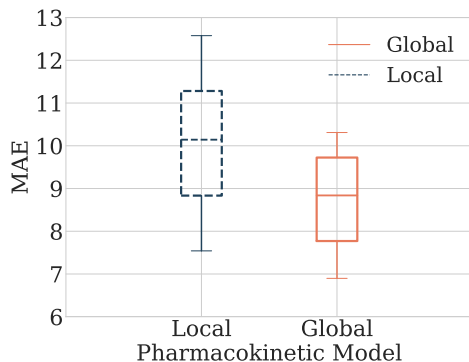


Figure 5: The boxplots show average MAE computed across 8 trials for global (orange) and local (blue) models for OhioT1DM subjects. Models trained on all subject data, or global models, have lower MAE, on average, than models trained on individual subjects, or local models.

glucose signal, static features, and exogenous features, consisting of insulin dose values. The sum total feature preprocessing approach was used to transform sparse features into non-sparse features of cumulative dose across an input window, as shown in Fig. 3.

3.4. Evaluation

Trained models were used to generate rolling window forecasts at one-step intervals. In accordance with prior work (Rubin-Falcone et al., 2022; Xie and Wang, 2020), we evaluate the blood glucose forecasts using two metrics: mean absolute error (MAE) and root mean squared error (RMSE) computed across 8 trials of individually trained models. Mathematical formulations for these metrics are provided in Appendix A.4. We evaluate model performance across all points within the specified time horizon. Furthermore, given the critical importance of healthcare outcomes related to blood glucose levels exceeding or falling below safe thresholds, we also assess the model’s performance exclusively at time points where blood glucose levels reach or fall below certain thresholds relevant to hypoglycemic and hyperglycemic events (i.e., ≤ 70 mg/dL and ≥ 180 mg/dL). For the OhioT1DM dataset, timestamps with forward-filled values were omitted from evaluation.

Our code implementation is open-source and can be found on Github. ¹

4. Results

The pharmacokinetic encoder significantly improves forecasting accuracy for the top performing deep

1. [Link will be added to camera-ready copy](#)

learning model by approximately 4.4% and 2.1%, for simulated and OhioT1DM datasets, respectively, as shown in Table 1. For the OhioT1DM dataset, the NHITS-Pharmacokinetic model has significantly smaller MAE than the NHITS-Sparse Exogenous model for forecasts evaluated at all values (t-test p-value: 4.44e-05) and critical values (t-test p-value: 1.6e-2). Fig. 6 demonstrates improved forecasting performance using the the NHITS-Pharmacokinetic model during hyperglycemic and hypoglycemic events for three randomly selected OhioT1DM subjects. Mean MAE and RMSE results with standard deviations computed across 8 trials are shown in Tables 7 and 8 in Appendix B.3.

We showcase the efficacy of our novel hybrid global-local model in producing more accuracy forecasts than models trained per patient. Global models consistently outperform local models, on average, for each OhioT1DM subject as shown in Table 4 and Fig. 9 in Appendix B.1. For the OhioT1DM dataset, the hybrid global-local pharmacokinetic model achieves a significantly lower (t-test p-value: 1.29e-2) MAE by 14.6% over patient-specific pharmacokinetic models. Fig. 5 shows that the global-local pharmacokinetic model has lower MAE, on average, across all OhioT1DM patients compared to the local models. Furthermore, the hybrid global-local pharmacokinetic model also achieves a significantly lower (t-test p-value: 3.83e-2) MAE by 9.2% over the patient-specific sparse exogenous models.

5. Discussion

Our pharmacokinetic encoder enables deep learning models to achieve significantly lower forecasting errors. As such, models that only include sparse features may be under-leveraging the potential utility of exogenous information. Our pharmacokinetic encoder can have multiple beneficial applications in clinical practice, such as issuing early warnings about unexpected treatment response, or helping to characterize patient-specific treatment effects in terms of drug absorption and elimination characteristics. The characterization of patient-specific pharmacokinetic parameters holds substantial potential for advancing the development of more effective treatments by tailoring medication to individual patients.

Assessing a forecasting model’s ability to effectively capture the impact of variables on the target signal is essential for ensuring the reliability of forecasts. We examine whether the pharmacokinetic model can

accurately capture the treatment effects of insulin on blood glucose by generating forecasts during time periods for three scenarios: with the original bolus insulin doses, with bolus insulin doses removed, and with bolus insulin doses increased by a factor of 10. When insulin doses are removed, blood glucose predictions increase, and when insulin doses are augmented, blood glucose predictions decrease as shown in Fig. 10 in Appendix B.2. Our model thus effectively learns the inhibitory treatment effects of insulin on blood glucose.

Bolus insulin is quick-acting and often taken before meals compared to basal insulin, which is longer-acting. Our pharmacokinetic encoder learns k_a values that align with this established knowledge. For OhioT1DM data, the average $k_{a_{bolus}}$ and $k_{a_{basal}}$ were **1.622** and **1.486**, respectively. For our approach, larger k_a values correspond to concentration curves with shorter duration, or steeper curves. The average k_a values for bolus insulin were higher than those for basal insulin, on average, resulting in shorter durations for bolus insulin concentration profiles.

To evaluate whether the difference in $k_{a_{bolus}}$ and $k_{a_{basal}}$ values was statistically significant, we compute a one-sided paired t-test of model-inferred k_a values for patients across the 8 trials. The alternative hypothesis claims that $k_{a_{bolus}}$ values are larger than $k_{a_{basal}}$. The test yielded a p-value of **0.043** indicating that the k_a parameter for bolus insulin is significantly higher than that for basal insulin when considering a significance level of 0.05. Thus, our approach can learn the relative differences in pharmacokinetic characteristics between basal and bolus insulin.

Limitations. We equate σ to our k_a parameter in the log-normal function and hold μ constant at 1. This simplification reduces the number of potential concentration curve shapes the model can learn. Tuning both σ and μ would enable more flexible concentration curves with potentially more accurate duration and peak characteristics, which could further improve forecasts.

Future Work. Future work will consider adaptations to the concentrator log-normal function to enable more flexible concentration curves. Future work will also consider expanding our pharmacokinetic encoder with functions relevant to other medication administration methods, such as intravenous injections. Finally, another interesting line of research is determining how to leverage the advantages of the global forecasting model with patient-specific k_a values for new patients.

Table 1: Mean absolute error (MAE) computed for model predictions across all values in the forecast horizon and only across critical values in the forecast horizon (blood glucose ≤ 70 | ≥ 180)

Simulated Dataset				
Model	All Values		Critical Values	
	Baseline	Exogenous	Baseline	Exogenous
ETS	10.040	–	13.531	–
MLP	9.734	8.653	12.189	9.887
LSTM	8.731	8.372	10.863	9.996
TCN	16.772	12.234	28.913	18.122
TFT	7.788	6.762	9.664	7.828
NHITS	8.333	7.282	10.184	8.353
TFT- Sum-Total	–	6.698	–	7.634
NHITS- Pharmacokinetic	–	7.027	–	7.917
TFT- Pharmacokinetic	–	6.466	–	7.514

OhioT1DM Dataset				
ETS	10.126	–	11.781	–
MLP	10.568	10.275	11.805	11.434
LSTM	10.604	9.606	12.999	11.144
TCN	11.011	11.090	12.693	13.212
TFT	9.605	9.515	10.686	10.555
NHITS	9.234	8.954	10.436	10.117
NHITS- Sum-Total	–	8.988	–	10.092
NHITS- Pharmacokinetic	–	8.769	–	10.007
TFT- Pharmacokinetic	–	9.492	–	10.484

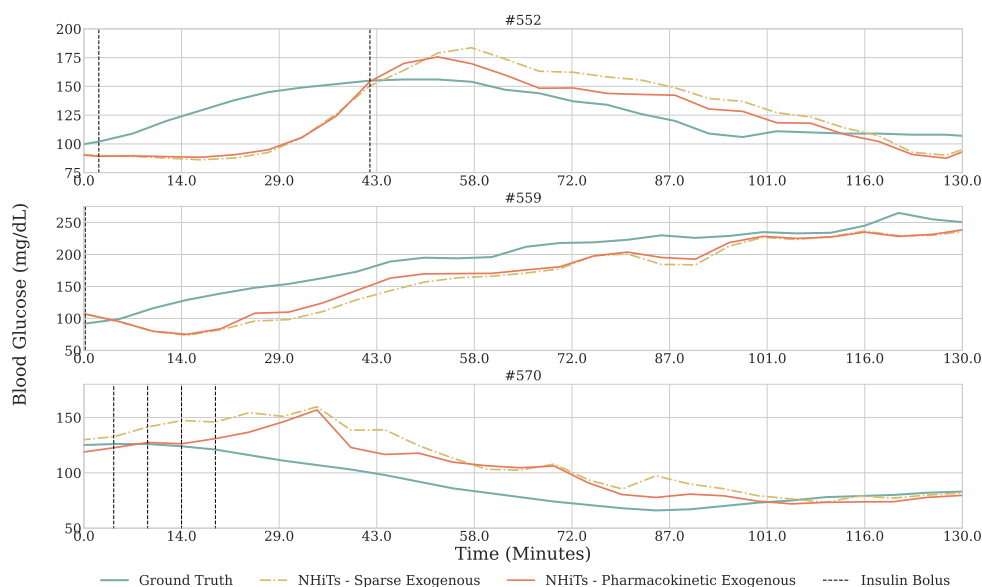


Figure 6: Blood glucose forecasts of the final horizon point for three OhioT1DM subjects. The NHITS - Pharmacokinetic model (orange) produces noticeably improved forecasts of the ground truth (blue) compared to the NHITS model with sparse exogenous features (yellow).

Acknowledgments

This work was partially supported by the NIH award R01HL141916. The authors wish to thank Dr. Frank Guyette, Dr. Leonard Weiss and Dr. Gilles Clermont for their guidance and informative conversations.

References

- James Arthur Harris and Francis Gano Benedict. *A biometric study of basal metabolism in man*. Carnegie institution of Washington, 21919.
- Shaojie Bai, J. Zico Kolter, and Vladlen Koltun. An empirical evaluation of generic convolutional and recurrent networks for sequence modeling, 2018.
- Christian Binder, Torsten Lauritzen, Ole Faber, and Stig Pramming. Insulin pharmacokinetics. *Diabetes care*, 7(2):188–199, 1984.
- Cristian Challu, Kin G. Olivares, Boris N. Oreshkin, Federico Garza, Max Mergenthaler-Canseco, and Artur Dubrawski. N-hits: Neural hierarchical interpolation for time series forecasting. In *AAAI-23*, 2022.
- Kyunghyun Cho, Bart van Merriënboer, Caglar Gulcehre, Dzmitry Bahdanau, Fethi Bougares, Holger Schwenk, and Yoshua Bengio. Learning phrase representations using rnn encoder-decoder for statistical machine translation, 2014.
- Matthew M Churpek, Richa Adhikari, and Dana P Edelson. The value of vital sign trends for detecting clinical deterioration on the wards. *Resuscitation*, 102:1–5, 2016.
- Jeffrey L. Elman. Finding structure in time. *Cognitive Science*, 14(2):179–211, 1990.
- Ian Fox, Lynn Ang, Mamta Jaiswal, Rodica Pop-Busui, and Jenna Wiens. Deep multi-output forecasting: Learning to accurately predict blood glucose trajectories. In *Proceedings of the 24th ACM SIGKDD international conference on knowledge discovery & data mining*, pages 1387–1395, 2018.
- Kunihiko Fukushima. Cognitron: A self-organizing multilayered neural network. *Biol. Cybernetics*, 20: 121–136, 1975.
- Federico Garza, Max Mergenthaler Canseco, Cristian Challú, and Kin G. Olivares. StatsForecast: Lightning fast forecasting with statistical and econometric models. PyCon Salt Lake City, Utah, US 2022, 2022. URL <https://github.com/Nixtla/statsforecast>.
- Stephen Gerry, Timothy Bonnici, Jacqueline Birks, Shona Kirtley, Pradeep S Virdee, Peter J Watkinson, and Gary S Collins. Early warning scores for detecting deterioration in adult hospital patients: systematic review and critical appraisal of methodology. *bmj*, 369, 2020.
- Rob Hyndman. *Forecasting with exponential smoothing: the state space approach*. Springer Berlin, Heidelberg, 2008.
- Maham Jahangir, Hammad Afzal, Mehreen Ahmed, Khawar Khurshid, and Raheel Nawaz. An expert system for diabetes prediction using auto tuned multi-layer perceptron. In *2017 Intelligent systems conference (IntelliSys)*, pages 722–728. IEEE, 2017.
- Diederik P. Kingma and Jimmy Ba. Adam: A method for stochastic optimization. In *3rd International Conference for Learning Representations*, 2017.
- Kezhi Li, John Daniels, Chengyuan Liu, Pau Herero, and Pantelis Georgiou. Convolutional recurrent neural networks for glucose prediction. *IEEE journal of biomedical and health informatics*, 24(2): 603–613, 2019.
- Bryan Lim, Serkan Ö. Arık, Nicolas Loeff, and Tomas Pfister. Temporal fusion transformers for interpretable multi-horizon time series forecasting. *International Journal of Forecasting*, 37(4):1748–1764, 2021.
- Cindy Marling and Razvan Bunescu. The ohiot1dm dataset for blood glucose level prediction: Update 2020. In *CEUR Workshop Proc*, 2020.
- Richard McShinsky and Brandon Marshall. Comparison of forecasting algorithms for type 1 diabetic glucose prediction on 30 and 60-minute prediction horizons. In *KDH@ ECAI*, pages 12–18, 2020.
- Vinod Nair and Geoffrey E. Hinton. Rectified linear units improve restricted boltzmann machines. In *ICML-23*, 2010.

- Kin G. Olivares, Cristian Challu, Grzegorz Marcjasz, Rafal Weron, and Artur Dubrawski. Neural basis expansion analysis with exogenous variables: Forecasting electricity prices with nbeatsx. *International Journal of Forecasting*, 39(2):884–900, 2022a.
- Kin G. Olivares, Cristian Challú, Federico Garza, Max Mergenthaler Canseco, and Artur Dubrawski. NeuralForecast: User friendly state-of-the-art neural forecasting models. PyCon Salt Lake City, Utah, US 2022, 2022b. URL <https://github.com/Nixtla/neuralforecast>.
- Boris N. Oreshkin, Dmitri Carпов, Nicolas Chapados, and Yoshua Bengio. N-BEATS: neural basis expansion analysis for interpretable time series forecasting. In *8th International Conference on Learning Representations, ICLR 2020*, 2020. URL <https://openreview.net/forum?id=r1ecqn4YwB>.
- Md Fazle Rabby, Yazhou Tu, Md Imran Hossen, Insup Lee, Anthony S Maida, and Xiali Hei. Stacked lstm based deep recurrent neural network with kalman smoothing for blood glucose prediction. *BMC Medical Informatics and Decision Making*, 21:1–15, 2021.
- Sara E. Rosenbaum. *Basic Pharmacokinetics and Pharmacodynamics: an Integrated Textbook and Computer Simulations*. Hoboken, New Jersey: John Wiley & Sons, Incorporated, 2017.
- Frank Rosenblatt. The perceptron: A probabilistic model for information storage and organization in the brain. *Psychological Review*, 65(6):386—408, 1958.
- Harry Rubin-Falcone, Ian Fox, and Jenna Wiens. Deep residual time-series forecasting: Application to blood glucose prediction. In *KDH@ ECAI*, pages 105–109, 2020.
- Harry Rubin-Falcone, Joyce M Lee, and Jenna Wiens. Forecasting with sparse but informative variables: A case study in predicting blood glucose. In *KDD '22: The 28th ACM SIGKDD Conference on Knowledge Discovery and Data Mining*. ACM, 2022. URL https://kdd-milets.github.io/milets2022/papers/MILETS_2022_paper_0765.pdf.
- Haşim Sak, Andrew Senior, and Françoise Beaufays. Long short-term memory based recurrent neural network architectures for large vocabulary speech recognition, 2014.
- Artemios-Anargyros Semenoglou, Evangelos Spiliotis, Spyros Makridakis, and Vassilios Assimakopoulos. Investigating the accuracy of cross-learning time series forecasting methods. *International Journal of Forecasting*, 37(3):1072–1084, 2021. ISSN 0169-2070. doi: <https://doi.org/10.1016/j.ijforecast.2020.11.009>. URL <https://www.sciencedirect.com/science/article/pii/S0169207020301850>.
- Slawek Smyl. A hybrid method of exponential smoothing and recurrent neural networks for time series forecasting. *International Journal of Forecasting*, 07 2019. doi: 10.1016/j.ijforecast.2019.03.017.
- Tue Søbørg, Christian Hove Rasmussen, Erik Mosekilde, and Morten Colding-Jørgensen. Bioavailability and variability of biphasic insulin mixtures. *European journal of pharmaceutical sciences*, 46(4):198–208, 2012.
- Aaron van den Oord, Sander Dieleman, Heiga Zen, Karen Simonyan, Oriol Vinyals, Alex Graves, Nal Kalchbrenner, Andrew Senior, and Koray Kavukcuoglu. Wavenet: A generative model for raw audio, 2016.
- Roberto Visentin, Chiara Dalla Man, and Claudio Cobelli. One-day bayesian cloning of type 1 diabetes subjects: Toward a single-day uva/padova type 1 diabetes simulator. *IEEE Transactions on Biomedical Engineering*, 63(11), 2016.
- Ruofeng Wen, Kari Torkkola, Balakrishnan Narayanaswamy, and Dhruv Madeka. A Multi-horizon Quantile Recurrent Forecaster. In *31st Conference on Neural Information Processing Systems NIPS 2017, Time Series Workshop*, 2017. URL <https://arxiv.org/abs/1711.11053>.
- Jinyu Xie. Simglucose v0.2.1 (2018), 2018. URL <https://github.com/jxx123/simglucose>.
- Jinyu Xie and Qian Wang. Benchmarking machine learning algorithms on blood glucose prediction for type i diabetes in comparison with classical time-series models. *IEEE Transactions on Biomedical Engineering*, 67(11):3101–3124, 2020. doi: 10.1109/TBME.2020.2975959.

Syed Mohammed Arshad Zaidi, Varun Chandola, Muhanned Ibrahim, Bianca Romanski, Lucy D Mastrandrea, and Tarunraj Singh. Multi-step ahead predictive model for blood glucose concentrations of type-1 diabetic patients. *Scientific Reports*, 11(1):24332, 2021.

Appendix A. First Appendix

A.1. Data

Fig. 7 shows the first 10 days of data for 6 subjects from the **simulated** dataset.

Fig. 8 shows the first 10 days of data for 6 subjects from the **OhioT1DM** dataset.

Table 2 shows sample count (% missing samples) for the original OhioT1DM datasets and preprocessed test set.

Table 2: Sample count (% missing samples) for the original OhioT1DM datasets and preprocessed test set

ID	Original		Preprocessed
	Train	Test	Test
540	13109 (8.87%)	3066 (6.43%)	2691 (6.91%)
544	12671 (16.16%)	3137 (13.42%)	2691 (14.08%)
552	11097 (18.80%)	3950 (40.15%)	2691 (53.36%)
559	12081 (10.64%)	2876 (12.59%)	2691 (13.45%)
563	13098 (7.44%)	2691 (4.50%)	2691 (4.50%)
567	13536 (19.78%)	2871 (16.79%)	2691 (16.91%)
570	11611 (5.42%)	2880 (4.69%)	2691 (4.91%)
575	13103 (9.44%)	2719 (4.74%)	269 (4.79%)
584	13248 (8.29%)	2995 (11.02%)	2691 (11.93%)
588	13105 (3.55%)	2881 (3.12%)	2691 (3.34%)
591	12755 (14.96%)	2847 (3.06%)	2691 (3.23%)
596	13630 (20.20%)	3003 (8.66%)	2691 (9.66%)

A.2. Models

Exponential Smoothing (ETS) The ETS model applies weighted average of past observations and

exponentially decreases weights for observations further into the past. (Hyndman, 2008).

Multi Layer Perceptrons (MLP) A neural network architecture composed of stacked Fully Connected Neural Networks trained with backpropagation (Nair and Hinton, 2010; Fukushima, 1975; Rosenblatt, 1958).

Neural Hierarchical Interpolation for Time Series (NHITS) - A deep learning model that applies multi-rate input pooling, hierarchical interpolation, and backcast residual connections together to generate additive predictions with different signal bands. The hierarchical interpolation technique promotes efficient approximations of arbitrarily long horizons and reduced computation (Challu et al., 2022).

Recurrent Neural Network (RNN) A recurrent neural network (RNN) architecture that applies recurrent transformations to obtain hidden states. The hidden states are transformed into contexts which are used as inputs to MLPs to generate forecasts. (Elman, 1990; Cho et al., 2014)

Long Short-Term Memory Recurrent Neural Network (LSTM) A recurrent neural network (RNN) architecture that transforms hidden states from a multilayer LSTM encoder into contexts which are used as inputs to MLPs to generate forecasts. (Sak et al., 2014)

Temporal Convolution Network (TCN) A 1D causal-convolutional network architecture that transforms hidden states into contexts which are used as inputs to MLP decoders to generate forecasts. To generate contexts, the prediction at time t is convolved only with elements from time t and earlier in the previous layer in what is referred to as causal convolutions (Bai et al., 2018; van den Oord et al., 2016).

Temporal Fusion Transformer (TFT) An attention-based deep learning architecture that learns temporal relationships at different scales using LSTMs for local processing and self-attention layers to model long-term dependencies. TFT also leverages variable selection networks as well as a series of gating layers to suppress unnecessary parts of the architecture (Lim et al., 2021).



Figure 7: Time series examples for the first 10 days of 6 subjects from the simulated dataset.

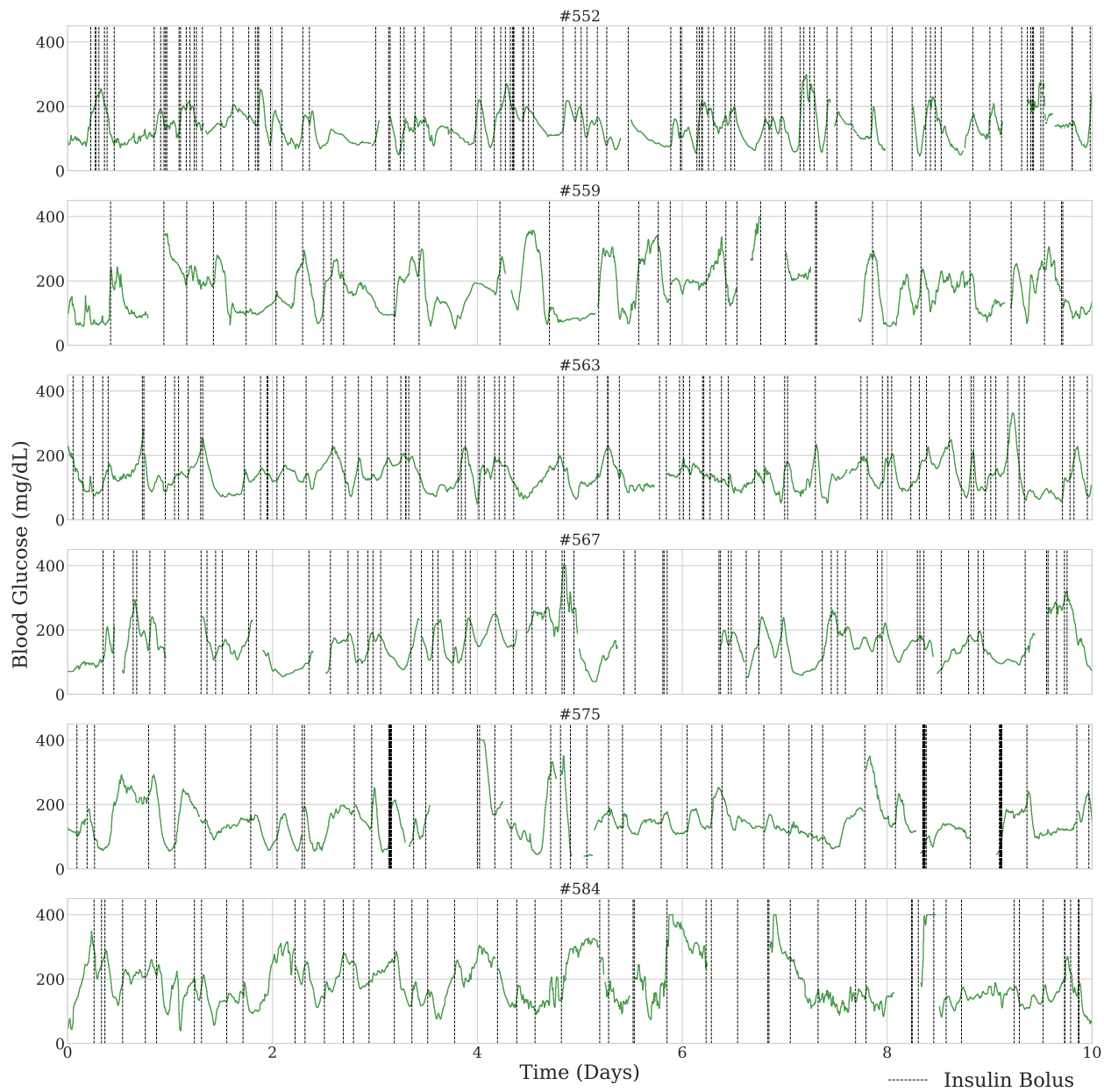


Figure 8: Time series for the first 10 days of 6 subjects from the OhioT1DM dataset.

A.3. Hyperparameters

For all baselines and our approach, we tune the learning rate, number of training iterations, batch size, dropout rate, and random seed, with values shown in table 3. Additionally, for all models with the Pharmacokinetic encoder, we tune the initial k_a values as shown in the second section of table 3.

Hyperparameter	Considered Values
Learning rate	Loguniform(1e-4, 1e-2)
Batch size	4
Dropout	{0.0, 0.1, 0.2, 0.3, 0.4, 0.5}
Training steps	{1000, 2000}
Random seed	DiscreteRange(1, 10)
Basal dose initial k_a	Uniform(1, 2, 11)
Bolus dose initial k_a	Uniform(1, 2, 11)

Table 3: Common hyperparameter search space

We tune additional specific hyperparameters for each architecture. For the MLP we tune the number of hidden units per layer ([128,256]); for the LSTM the hidden size ([128,256]); for the TCN the hidden size ([128,256]) and number of dilations ([2,4,8]); for the TFT the hidden size ([128,256]); for the NHITS we did not tune additional hyperparameters. The replicable experiments with the full set of hyperparameters for each architecture are included in the paper’s code.

A.4. Metrics

Mean Absolute Error (MAE)

$$MAE(y_{t+1,t+H}, \hat{y}_{t+1,t+H}) = \frac{1}{H} \sum_{i=t+1}^{t+H} |y_i - \hat{y}_i|$$

Root Mean Square Error (RMSE)

$$RMSE(y_{t+1,t+H}, \hat{y}_{t+1,t+H}) = \sqrt{\frac{1}{H} \sum_{i=t+1}^{t+H} (y_i - \hat{y}_i)^2}$$

Appendix B. Second Appendix

B.1. Patient-specific (local) models

We showcase the effectiveness of global models, with parameters shared across subjects, in generating more accuracy forecasts compared to local models trained for individual subjects. Global models consistently outperform local models, on average across

8 trials, for each OhioT1DM subject as shown in Table. 4 and Fig 9b. Furthermore, the global NHITS-Pharmacokinetic model consistently outperforms the global NHITS-Exogenous model, on average, for each OhioT1DM subject as shown in Fig 9a.

Table 4: MAE computed across forecast horizon values using local and global models.

ID	Exogenous		Pharmacokinetic	
	Local	Global	Local	Global
540	11.358 (0.236)	10.325 (0.168)	12.059 (0.414)	10.050 (0.150)
544	7.513 (0.207)	7.312 (0.150)	7.839 (0.239)	7.028 (0.127)
552	8.400 (0.346)	7.547 (0.105)	8.854 (0.282)	7.308 (0.150)
559	9.888 (0.379)	9.093 (0.094)	10.486 (0.579)	9.000 (0.065)
563	9.247 (0.102)	8.610 (0.071)	9.172 (0.302)	8.580 (0.107)
567	11.254 (0.534)	9.835 (0.142)	11.455 (0.349)	9.662 (0.181)
570	8.160 (0.318)	7.470 (0.134)	8.259 (0.511)	7.280 (0.160)
575	10.500 (0.166)	9.734 (0.086)	11.149 (0.377)	9.539 (0.136)
584	10.605 (0.332)	9.958 (0.146)	13.706 (6.499)	9.787 (0.135)
588	8.966 (0.258)	8.295 (0.041)	9.454 (0.297)	8.158 (0.077)
591	11.237 (0.321)	10.344 (0.080)	11.275 (0.102)	10.103 (0.075)
596	8.797 (0.125)	8.230 (0.073)	9.471 (0.624)	8.008 (0.136)
All	9.661 (1.272)	8.954 (0.058)	10.265 (1.651)	8.769 (0.069)

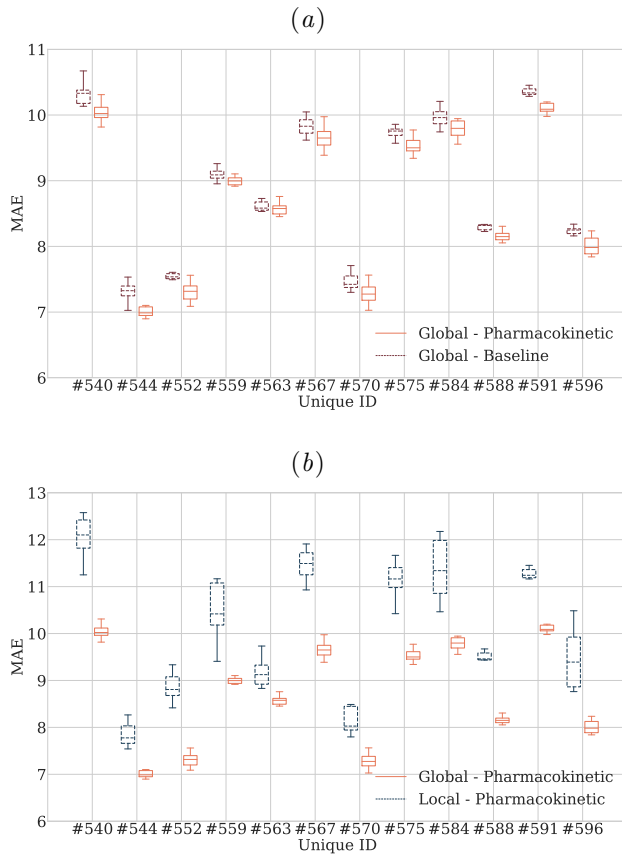


Figure 9: The pharmacokinetic NHITS model outperforms the NHITS baseline exogenous model across all patients, on average (a). Additionally, the pharmacokinetic model trained on data from subjects, or the global model, achieves lower MAE than models trained on individual subjects, or local models (b).

B.2. Forecasting treatment effects

In this appendix, we explore the effect of changing the insulin dosage on the forecasts produced by our approach. Fig. 10, demonstrates that the pharmacokinetic model appropriately learns the treatment effect of insulin on blood glucose for OhioT1DM subjects, decreasing the forecast when the dosage increases.

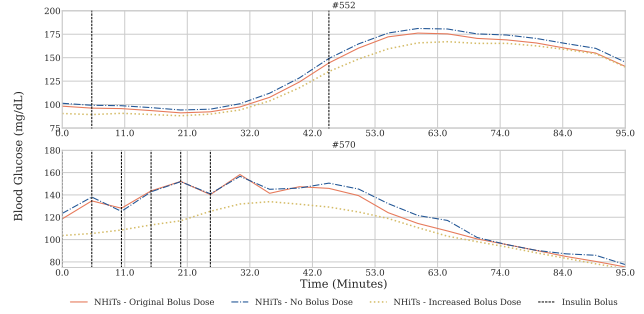


Figure 10: Treatment effect of insulin on the NHITS pharmacokinetic model. Each point in the plot corresponds to the final horizon point. Forecasts with original bolus doses (orange), removing bolus insulin doses results in higher forecasts (blue), and augmenting doses results in lower blood glucose forecasts (yellow).

B.3. Model MAE and RMSE results

This appendix presents the complete results for all models, metrics of evaluation, and both simulated data and OhioT1DM. Standard deviation across 8 trials are provided in parenthesis.

Table 5: Mean absolute error (MAE) computed for model predictions across all values in the forecast horizon and only across critical values in the forecast horizon (blood glucose ≤ 70 | ≥ 180) for **simulated** data. Average results are computed across 8 trials.

Model	All Values		Critical Values	
	Baseline	Exogenous	Baseline	Exogenous
ETS	10.040 (0.00)	–	13.531 (0.00)	–
MLP	9.734 (1.125)	8.653 (1.500)	12.189 (1.198)	9.887 (1.681)
LSTM	8.731 (0.573)	8.372 (1.553)	10.863 (1.555)	9.996 (2.315)
TCN	16.772 (9.795)	12.234 (7.866)	28.913 (23.303)	18.122 (19.911)
TFT	7.788 (1.599)	6.762 (0.570)	9.664 (1.999)	7.828 (0.752)
NHITS	8.333 (0.166)	7.282 (0.184)	10.184 (0.303)	8.353 (0.363)
TFT-Sum Total	–	6.698 (0.508)	–	7.634 (0.546)
NHITS-Pharmacokinetic	–	7.027 (0.091)	–	7.917 (0.268)
TFT-Pharmacokinetic	–	6.466 (0.570)	–	7.514 (0.985)

Table 6: Root Mean Square error (RMSE) computed for model predictions across all values in the forecast horizon and only across critical values in the forecast horizon (blood glucose ≤ 70 | ≥ 180) for **simulated** data.

Model	All Values		Critical Values	
	Baseline	Exogenous	Baseline	Exogenous
ETS	15.754 (0.00)	–	23.151 (0.00)	–
MLP	14.285 (0.981)	11.607 (1.756)	19.443 (0.737)	13.731 (2.321)
LSTM	12.802 (0.759)	11.273 (1.918)	16.903 (2.100)	13.595 (3.260)
TCN	22.874 (11.937)	16.194 (10.309)	36.468 (22.454)	22.533 (20.991)
TFT	11.930 (1.424)	9.801 (0.690)	15.736 (1.676)	11.708 (0.948)
NHITS	13.058 (0.255)	10.479 (0.372)	18.036 (0.644)	12.822 (0.855)
TFT-Sum Total	–	9.711 (0.599)	–	11.283 (0.748)
NHITS-Pharmacokinetic	–	10.024 (0.204)	–	11.931 (0.549)
TFT-Pharmacokinetic	–	9.407 (0.654)	–	11.224 (1.152)

Table 7: Mean absolute error (MAE) computed for model predictions across all values in the forecast horizon and only across critical values in the forecast horizon (blood glucose ≤ 70 | ≥ 180) for **OhioT1DM** data. Average results are computed across 8 trials.

Model	All Values		Critical Values	
	Baseline	Exogenous	Baseline	Exogenous
ETS	10.126 (0.00)	–	11.781 (0.00)	–
MLP	10.568 (0.628)	10.275 (0.183)	11.805 (0.731)	11.434 (0.186)
LSTM	10.604 (0.929)	9.606 (0.372)	12.999 (2.294)	11.144 (0.708)
TCN	11.011 (1.066)	11.090 (0.708)	12.693 (1.334)	13.212 (0.886)
TFT	9.605 (0.735)	9.515 (0.310)	10.686 (0.986)	10.555 (0.495)
NHITS	9.234 (0.056)	8.954 (0.058)	10.436 (0.125)	10.117 (0.086)
NHITS-Sum Total	–	8.988 (0.023)	–	10.092 (0.082)
NHITS-Pharmacokinetic	–	8.769 (0.069)	–	10.007 (0.087)
TFT-Pharmacokinetic	–	9.492 (0.399)	–	10.484 (0.374)

Table 8: Root mean square error (RMSE) computed for model predictions across all values in the forecast horizon and only across critical values in the forecast horizon (blood glucose ≤ 70 | ≥ 180) for **OhioT1DM** data.

Model	All Values		Critical Values	
	Baseline	Exogenous	Baseline	Exogenous
ETS	15.351 (0.00)	–	17.478 (0.00)	–
MLP	16.128 (0.580)	15.625 (0.131)	17.942 (0.716)	17.482 (0.232)
LSTM	15.766 (0.930)	14.704 (0.297)	18.565 (1.818)	16.784 (0.688)
TCN	16.173 (0.932)	16.192 (0.545)	18.432 (1.097)	18.978 (0.806)
TFT	15.031 (0.576)	14.820 (0.186)	16.720 (0.954)	16.455 (0.413)
NHITS	15.106 (0.075)	14.596 (0.080)	16.901 (0.168)	16.421 (0.133)
NHITS-Sum Total	–	14.714 (0.043)	–	16.438 (0.135)
NHITS-Pharmacokinetic	–	14.375 (0.126)	–	16.287 (0.154)
TFT-Pharmacokinetic	–	14.846 (0.366)	–	16.351 (0.284)